Sensors & Actuators: B. Chemical 279 (2019) 213–222

Contents lists available at ScienceDirect

Sensors and Actuators B: Chemical

journal homepage: www.elsevier.com/locate/snb

Highly selective and stable mixed-potential type gas sensor based on stabilized zirconia and $Cd_2V_2O_7$ sensing electrode for NH_3 detection

Fangmeng Liu[a], Siqi Li[a], Junming He[a], Jing Wang[a], Rui You[b], Zijie Yang[a], Lianjing Zhao[a], Peng Sun[a], Xu Yan[a], Xishuang Liang[a], Xiaohong Chuai[a,*], Geyu Lu[a,*]

[a] State Key Laboratory on Integrated Optoelectronics, Key Laboratory of Advanced gas sensors, Jilin Province, College of Electronic Science and Engineering, Jilin University, 2699 Qianjin Street, Changchun 130012, China
[b] Department of Precision Instrument, Tsinghua University, Beijing 100084, China

ARTICLE INFO

Keywords:
NH_3 sensor
Stabilized zirconia
$Cd_2V_2O_7$
Mixed potential

ABSTRACT

In this work, the highly selective and stable mixed potential type stabilized zirconia (YSZ) based gas sensor using $Cd_2V_2O_7$ sensing electrode (SE) synthesized via simple coprecipitation method was fabricated and developed for effective detection of NH_3 at 650 °C. The as-prepared $Cd_2V_2O_7$ sensing material was characterized by X-ray diffraction (XRD), Raman spectrum, X-ray photoelectron spectroscopy (XPS) and Field-emission scanning electron microscopy (FESEM). The results of gas sensing measurement indicated that the sensor attached with $Cd_2V_2O_7$- SE displayed the response value of −68 mV and rapid response rate of 5 s to 100 ppm NH_3 at 650 °C. The present device also exhibited the low detection limit of 1 ppm and the piecewise sensitivities of −6 and −66 mV/decade to NH_3 in the concentration ranges of 1–10 ppm and 10–200 ppm, respectively. Moreover, the fabricated sensor showed good reproducibility, excellent selectivity, stability to oxygen concentration, relative humidity and 30 days continuous aging of high temperature at 650 °C. And the complex impedance and polarization curves were performed to explain the selectivity and verify the sensing mechanism involving mixed potential model.

1. Introduction

The atmospheric pollution problem is becoming more and more prominent with the acceleration of industrialization and urbanization. Among various air pollutions, the NO_x (NO_2 or NO) comes from the operation mode of the automotive vehicle which is driven in lean conditions are the major and the most harmful air pollutions, due to NO_x not only cause the ozone hole and damage directly the health of human bodies but also produce acid rain, photochemical smog, greenhouse effect and other environmental disaster [1–4]. Generally, employment of selective catalytic reduction (SCR) system based on urea-water solution as catalyst is the faithful technologies of exhaust gas after-treatment system to achieve effectively NO_x conversion in the automotive engines, especially heavy duty diesels [5,6]. In the process of catalytic reaction, as shown in Eqs. (1)–(3), the urea-water solution is decomposed to ammonia (NH_3), and the NO_x gases are reduced with NH_3 to generate the harmless substances of N_2 and H_2O [7]. However, in order to accurately remove the NO_x in exhaust gases and prevent the uncontrolled redundant NH_3 leakage to achieve the actual closed loop feedback control, the high performance NH_3 sensor for on-board diagnosis (OBD) is advantageous and essential to monitor the NH_3 concentration in exhaust gases downstream of SCR system. Considering the harsh operating environment (high temperature, high humidity, long-term operation, high selectivity and stability) of on-board gas sensor, the mixed potential type sensing device based on stabilized zirconia (YSZ) solid electrolyte and metal oxide sensing electrode is regarded as one of the most promising candidate in NH_3 detection of automobile exhaust gas.

$$NH_2CONH_2 + H_2O(stream) \rightarrow 2NH_3 + CO_2 + H_2O \quad (1)$$

$$4NH_3 + 2NO_2 + 2NO \rightarrow 4N_2 + 6H_2O \quad (2)$$

$$4NH_3 + 2NO + O_2 \rightarrow 4N_2 + 6H_2O \quad (3)$$

The research on enhanced YSZ-based gas sensor involving in mixed potential sensing mechanism was mainly focused on the development of novel sensing electrode material with high electrochemical catalytic activity, the fabrication of high performance three phase boundary (TPB) and construction of new device structure [8–14]. The electrochemical reactions for mixed potential type gas sensor based on YSZ

* Corresponding authors.
E-mail addresses: xhchuai@jlu.edu.cn (X. Chuai), lugy@jlu.edu.cn (G. Lu).

https://doi.org/10.1016/j.snb.2018.09.024
Received 22 April 2018; Received in revised form 22 August 2018; Accepted 6 September 2018
Available online 07 September 2018
0925-4005/

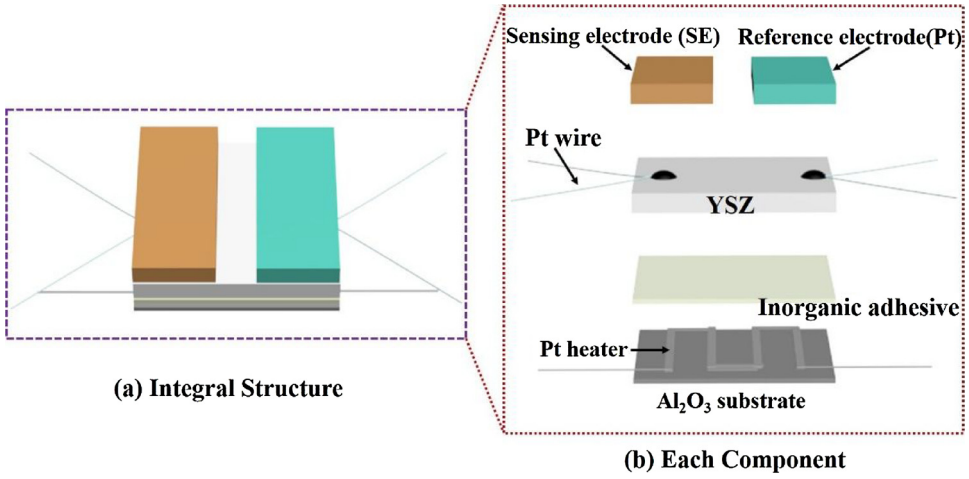

Fig. 1. Schematic diagram of the integral structure (a) and each component (b) for the fabricated sensor.

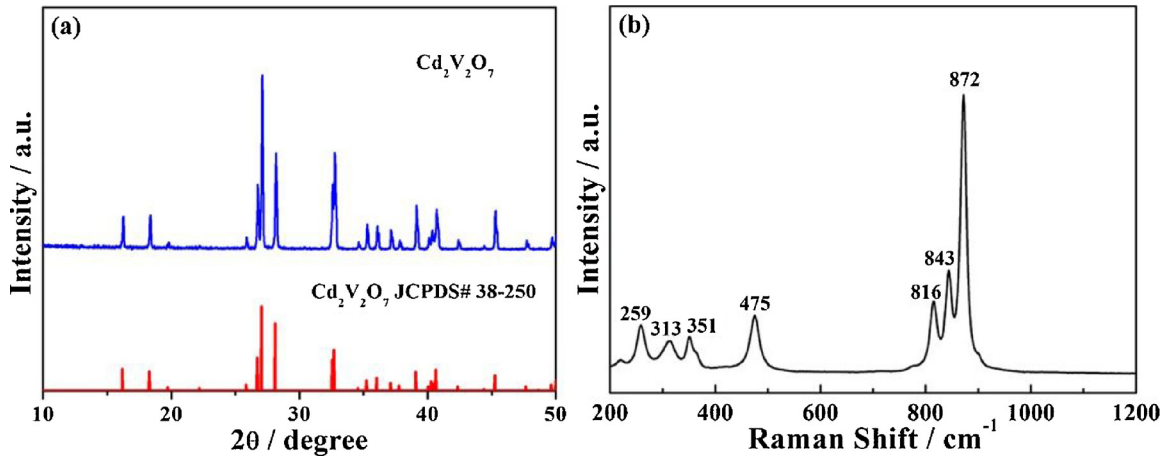

Fig. 2. (a) XRD pattern and (b) Raman spectrum of $Cd_2V_2O_7$ sensing electrode material.

electrolyte occurred at TPB of sensing electrode-YSZ-target gas, thus selection of a sensing material with excellent electrochemical activity is the key factor to get high performance sensing device. Up to now, various sensing electrode materials, such as Au/NiO [15], V_2O_5-WO_3-TiO_2 [16], $CoWO_4$ [17], $Ni_3V_2O_8$ [18], $CoFe_2O_4$ [19] have been developed and are used for fabricating high performance NH_3 sensor based on mixed potential mode. Therefore, based on previous research work, how to further develop new sensing material with high performance and extend the system scope of sensing electrode material is inevitable to expand the mixed potential type YSZ-based NH_3 sensor camp.

Interestingly, bimetallic oxide systems with multiple functionalities presented prominent catalytic activity, selectivity and stability over monometallic oxide materials, and was the important path for design of high performance sensing material. As reported in literatures [20,21], for the heterogeneous catalysis of vanadium oxides, redox property and surface acidity depend strongly on the additives or support oxide materials. Thus, the design of bimetallic oxide material based on the vanadium oxides can be a suitable sensing material to sensitive and selective detect NH_3 by the addition of additive metal cations. In this work, a new vanadium-based composite oxide sensing material ($Cd_2V_2O_7$) was prepared via facile coprecipitation method and used for highly selective and stable detection of NH_3 for YSZ-based mixed potential type gas sensor. The detailed sensing characteristics of the fabricated device were investigated and the sensing mechanism was proposed and discussed.

2. Experimental

2.1. Synthesis and characterization of the $Cd_2V_2O_7$ sensing electrode material

The Cadmium vanadate ($Cd_2V_2O_7$) sensing electrode material was successfully synthesized via the coprecipitation method from Cd $(NO_3)_2{\cdot}4H_2O$ and NH_4VO_3 as the starting materials. Typically, 3 mmol of $Cd(NO_3)_2{\cdot}4H_2O$ and NH_4VO_3 were dissolved in a certain amount of deionized water and stirred at 80 °C for 2 h. Then, ammonia hydroxide solution was dropwise added with constant stirring to the above solution until the pH value was up to 8 to obtain precipitate. The precipitate was filtered, washed using deionized water and ethanol solution and then the resultant precursor product was maintained at 80 °C for 12 h in vacuum drying oven. Finally, the dry product was sintered at 800 °C in muffle furnace for 2 h to get $Cd_2V_2O_7$ sensing material.

X-ray diffraction (XRD) pattern of $Cd_2V_2O_7$ material is characterized by Rigaku wide-angle X-ray diffractometer (D/max rA, using Cu Kα radiation at wave length = 0.1541 nm) in the angular range of 10–50°. Raman spectroscopy of the sensing material is recorded using LabRAM HR Evolution spectrometer with a laser wavelength of 532 nm. Field-emission scanning electron microscopy (FESEM) observation of surface morphology of $Cd_2V_2O_7$-SE is measured using a JEOL JSM- 6500 F microscope with an accelerating voltage of 15 kV. X-ray photoelectron spectroscopy (XPS) measurement of as-prepared material is performed on a Thermo ESCALAB250 spectrometer equipped with an Al-Kα ray source.

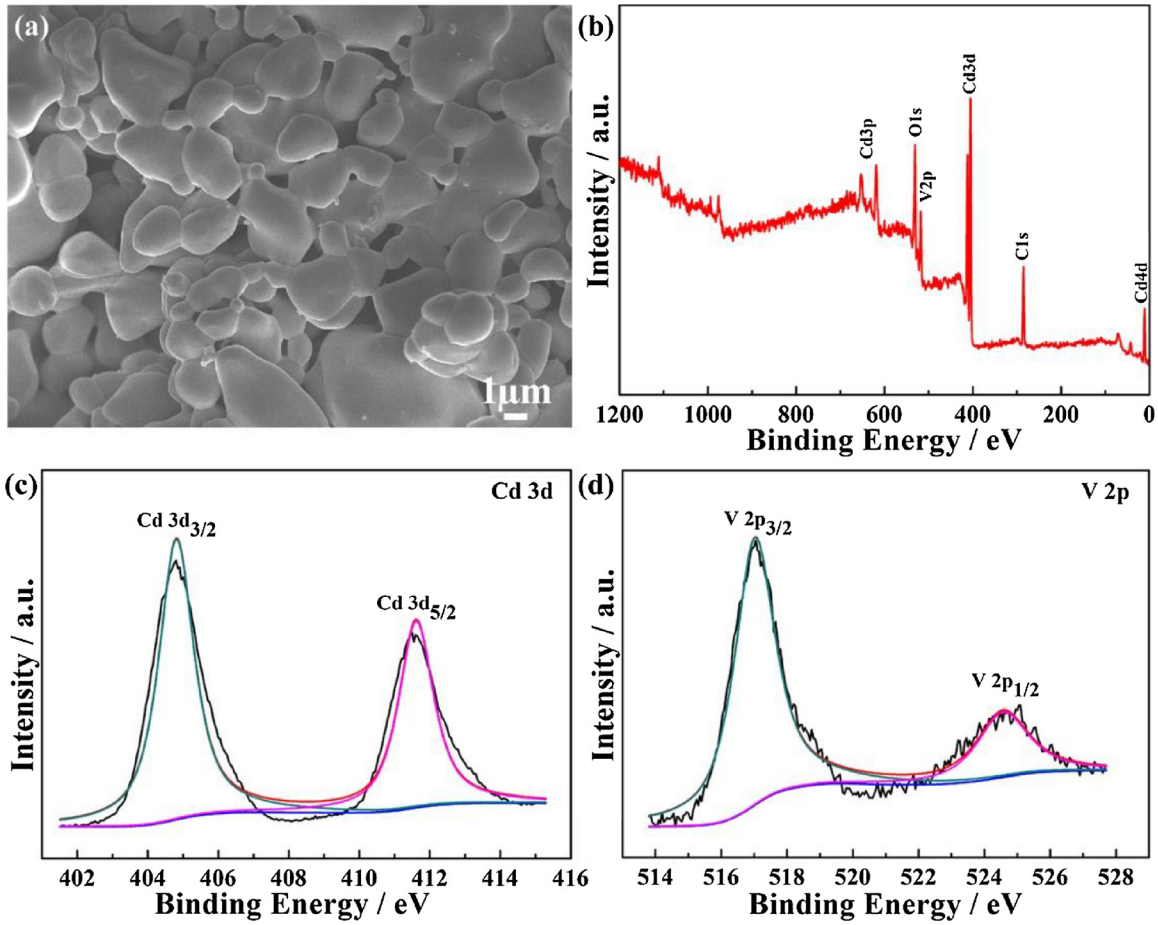

Fig. 3. SEM image of $Cd_2V_2O_7$-SE (a) and XPS spectra of $Cd_2V_2O_7$ composite material (b) survey; (c) Cd 3d; (d) V 2p.

2.2. Fabrication and measurement of the sensor

Fig. 1 depicts a schematic diagram of the integral structure and each component for the fabricated sensor. The sensor was fabricated using the YSZ substrate (8 mol% Y_2O_3-doped, 2 mm × 2 mm square, 0.3 mm thickness, provided by Anpeisheng Corp., China). A point-shaped and a narrow stripe-shaped Pt electrode (Reference electrode, RE) with Pt wire were performed on two ends of the YSZ substrate using commercial Pt paste (Sino-platinum Metals Co., Ltd.) and were sintered at 1000 °C. The $Cd_2V_2O_7$ sensing material was mixed with a minimum quantity of deionized water to get sensing electrode paste and then the paste was deposited on the point-shaped Pt with a fine brush to form stripe-shaped SE on the upper surface of YSZ substrate, and the device was co-fired at 800 °C for 2 h to gain good contact between SE and YSZ substrate. Subsequently, the Pt heater formed on Al_2O_3 substrate was fixed on the bottom of the YSZ substrate using the inorganic adhesive, which provided the required working temperature by applying the current. The gas sensing performance of the fabricated sensor was measured by a conventional static method [22,23]. The electric potential difference between the SE and the RE was measured with a digital electrometer (Rigol. DM3054) when the sensor was exposed to air or sample gases. The test results were recorded with a computer connected to the electrometer. In order to assure the accuracy of measurement result, the test times in air and different concentrations of sample gases are kept consistent and the response signal exposed to sample gas at the last second as the calibration of response value. The current-voltage (polarization) curves of sensors were performed utilizing the potentiodynamic method (CHI600C, Instrument corporation of Shanghai, China) based on a two-electrode configuration in air, 50, 100 and 200 ppm NH_3 at 650 °C. The complex impedance measurements of the sensor in air and various tested gases were performed by using an impedance analyzer (Solartron 1260 and Solartron 1287) with the amplitude of the AC potential signal at 300 mV in the frequency range of 1 MHz–0.1 Hz at 650 °C.

3. Results and discussion

The crystalline structure and purity of as-prepared sensing material was investigated by XRD measurement. Fig. 2**(a)** displays the XRD pattern of prepared $Cd_2V_2O_7$ sensing electrode material and the result demonstrated that all diffraction peaks of as-prepared material were in correspondence with the monoclinic $Cd_2V_2O_7$ (JCPDS 38-250). No other diffraction peaks of the sensing material have been observed, indicating the high purity. Raman spectrum of $Cd_2V_2O_7$ sensing electrode material is presented in Fig. 2**(b)**. The vibrational modes with high frequencies at around 872, 843 and 816 cm^{-1} were associated with V—O stretching mode, stretching vibrations of VO_3 group in $(V_2O_7)^{4+}$ ions and stretching vibrations of the V—O—V bridges in $Cd_2V_2O_7$, in agreement with previous reports [24,25]. And the modes with low frequency positions located at 475, 351, 313 and 259 cm^{-1} were assigned to symmetry related vibrations of $Cd_2V_2O_7$ [26].

The morphology and microstructure of $Cd_2V_2O_7$-SE were further characterized by FESEM. As shown in Fig. 3**(a)**, the micro-sized particles of sensing material were obtained, and the loose and porous microstructure of SE was observed, which contributed to the diffusion of target gas in sensing electrode layer. The chemical state and compositions information of as-prepared $Cd_2V_2O_7$ sensing material was further evaluated by performing X-ray photoelectron spectroscopy (XPS). From the survey spectrum of $Cd_2V_2O_7$ in Fig. 3**(b)**, it can be clearly seen that the Cd, V, O and C elements were existed in the prepared sensing

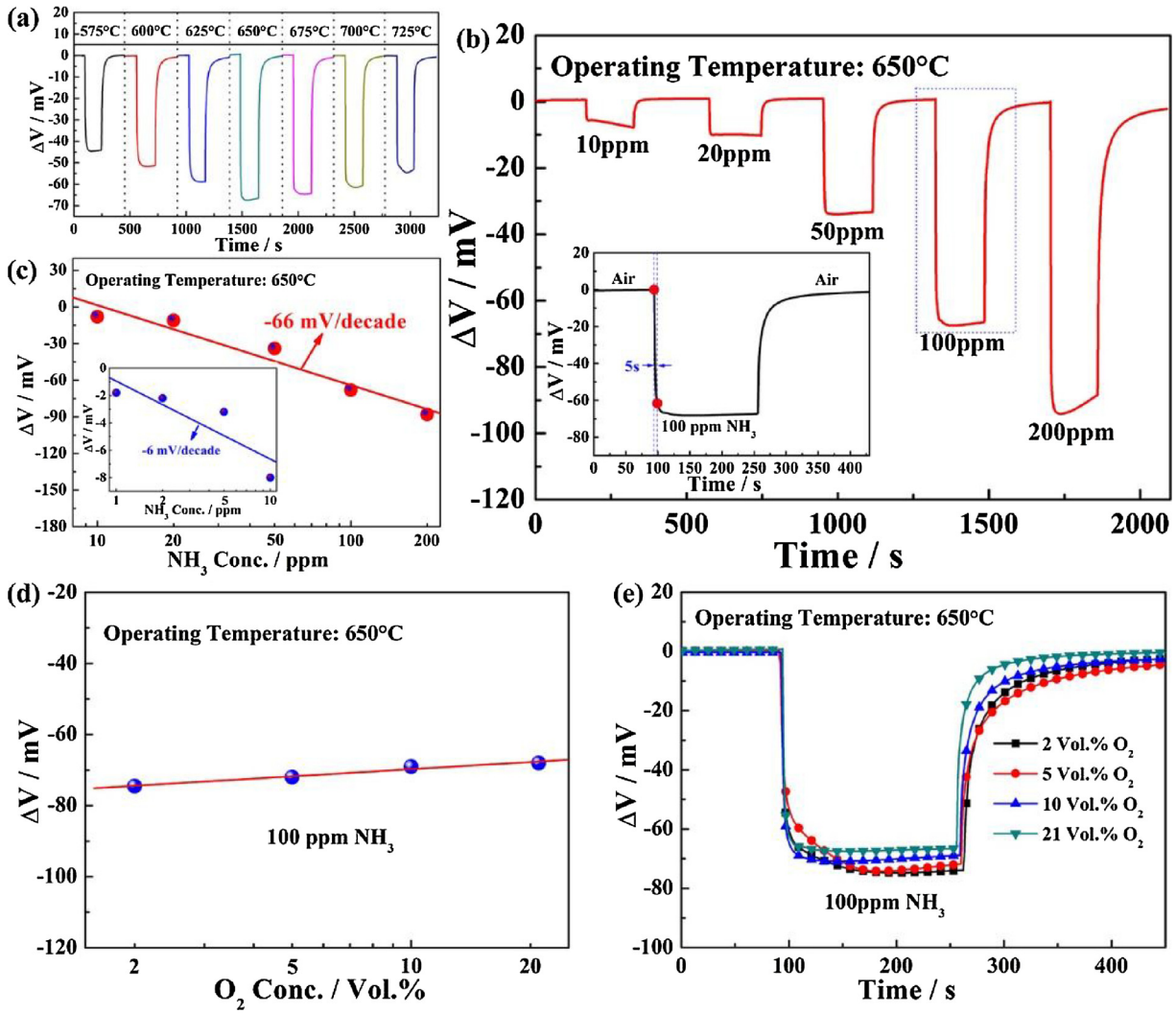

Fig. 4. (a) Response and recovery curves of the sensor utilizing $Cd_2V_2O_7$-SE to 100 ppm NH_3 at different operating temperatures; (b) Response transients for the sensor toward 10–200 ppm NH_3 at 650 °C; (c) Dependence of ΔV on the logarithm of NH_3 concentrations for the sensor at 650 °C; (d, e) Response of the sensor to 100 ppm NH_3 at different concentrations of O_2.

Table 1
Comparison of the sensing performance of the present sensor and that of devices reported in literatures.

Material	Operating Temperature (°C)	NH_3 Conc. (ppm)	Sensor Response (mV)	Ref.
NiO/Au	800	100	–34	[15]
$CuNb_2O_6$	300	500	56	[36]
$CoWO_4$	700	100	–8	[17]
Pt-WO_3	350	4000	45	[37]
Bi_2O_3	600	500	68.2	[38]
$Ni_3V_2O_8$	650	100	–62	[18]
Au-SnO_2	650	100	–63	[11]
$CoFe_2O_4$	450	320	81	[19]
$Cd_2V_2O_7$	650	100	–68	This work

material. The standardized C 1 s binding energy (284.6 eV) was used as reference calibration for all other peaks. Fig. 3**(c and d)** presents the high-resolution scanning XPS spectrum of Cd 3d and V 2p of $Cd_2V_2O_7$ material. The two peaks appeared at binding energies of 404.8 eV and 411.6 eV were the characteristic of Cd $3d_{3/2}$ and Cd $3d_{5/2}$, which were consistence with Cd^{2+} [27,28] (Fig. 3c). The obvious two peaks located at 517 eV and 524.6 eV were attributed to $V2p_{3/2}$ and $V2p_{1/2}$, which is indexed to V^{5+} in $Cd_2V_2O_7$ [29,30] (Fig. 3d).

The gas sensing properties of the sensor based on YSZ and metal oxide sensing electrode were heavily relied on the working temperature. Thus, the influence of the operating temperature for the sensor attached with $Cd_2V_2O_7$-SE on response to 100 ppm NH_3 were evaluated and shown in Fig. 4**(a)**. Obviously, the maximum response value of fabricated sensor to 100 ppm NH_3 was achieved at 650 °C, which was considered as the optimal operating temperature. Thus, the detailed gas sensing performances of the developed sensor using $Cd_2V_2O_7$-SE were comprehensive studied in an upcoming section. Fig. 4**(b)** shows the response transients for the sensor to 10–200 ppm NH_3 at 650 °C. The present sensor exhibited the good response and recovery characteristics to different concentrations of NH_3 and the response value presented progressive increase trend with the increase of target gas concentration. The response value and 90% response time for the fabricated device to 100 ppm NH_3 were −68 mV and 5 s at 650 °C, which indicated the high perception signal and response rate. Additionally, the sensor displayed the low detection limit of 1 ppm to NH_3 and piecewise negative linear relationship between response value and logarithm of NH_3 concentrations in the range of 1–200 ppm, which the sensitivities to 1–10 ppm and 10–200 ppm NH_3 were –6 and −66 mV/decade at 650 °C, respectively (Fig. 4**(c)**). According to the mixed potential type sensing mechanism reported by Miura and other researchers [18,31–33], the NH_3 sensitivity of the fabricated sensor can be determined by the degree of

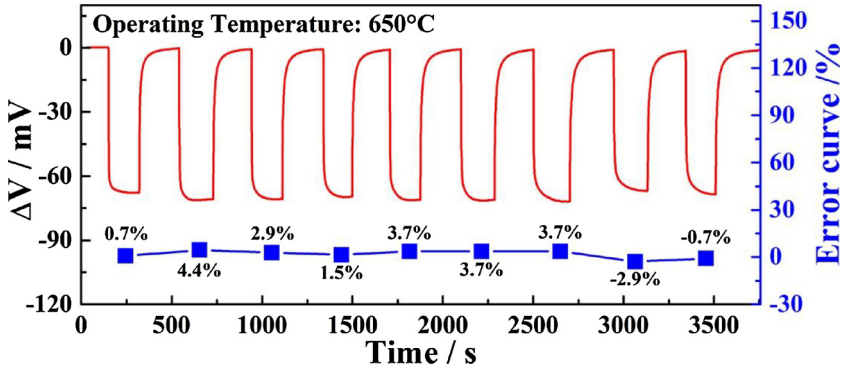

Fig. 5. Continuous response and recovery transients of the sensor using $Cd_2V_2O_7$-SE to 100 ppm NH_3 at 650 °C.

gas phase catalytic reaction of NH_3 in the $Cd_2V_2O_7$ layer and the electrochemical catalytic reaction at TPB of $Cd_2V_2O_7$/YSZ/NH_3. The NH_3 gas is consumed in the diffusion process of the SE layer ($4NH_3 + 3O_2 \rightarrow 2N_2 + 6H_2O$), and the unreacted NH_3 gas arrived at the TPB to participate in electrochemical anodic and cathodic reactions. When the present device was measured at the lower concentration range of NH_3, the NH_3 consumption proportion accounted for total quantity of NH_3 in the diffusion process is larger than that of higher concentration range of NH_3. In this regard, the NH_3 concentration proportion participated in the electrochemical reaction at TPB in the lower concentration range was obviously less than that of higher NH_3 concentration. The NH_3 consumption process induced by gas phase catalytic reaction in $Cd_2V_2O_7$ layer may induce to the piecewise sensitivities to NH_3 [34,35]. However, the low detection limit of 1 ppm to NH_3 for the fabricated device is determined by the degree of electrochemical anodic reaction of NH_3 arrived at TPB and electrochemical cathodic reaction of O_2. Comparison of the sensing performance of the present fabricated sensor and that of reported in literatures, as exhibited in Table 1. The present sensing device displayed the better superiority in NH_3 sensing properties than other developed sensors in literatures. Moreover, the influence of oxygen partial pressure on NH_3 sensing property is investigated and the test results are exhibited in Fig. 4**(d and e)**. As seen, the response value of the fabricated device to 100 ppm NH_3 presented positive linear variety with the logarithm of O_2 concentrations in the range of 2–21 Vol.% at 650 °C. The response signal of the sensor to 100 ppm NH_3 increased slightly with the decrease of oxygen concentration and the maximum change degree of response value to 100 ppm NH_3 was 9.6%, which exhibited good stability in different concentrations of oxygen partial pressure.

Fig. 5 reveals the continuous response and recovery transients of the sensor using $Cd_2V_2O_7$-SE to 100 ppm NH_3 at 650 °C. The change of response is denoted by $(\Delta V_{other}-\Delta V_0)/\Delta V_0 \times 100\%$, where ΔV_{other} and ΔV_0 represent the ΔV of the sensor in other cycles and −68 mV, respectively. We can clearly see that the response and recovery characteristics of the developed device to 100 ppm NH_3 hold good consistence during the continuous nine cycles measurement and the maximum change of the response value to 100 ppm NH_3 was 4.4% at 650 °C, which represented the favorable reproducibility to NH_3. Additionally, the fabricated sensing device is always confronted with other interference gases or multiple coexistence gases in the actual working condition, thus, the measurement and evaluation of selectivity for the present sensor are absolutely necessary. The sensor attached with $Cd_2V_2O_7$-SE was exposed to various gases at 650 °C and the measured response and recovery curves are depicted in Fig. 6**(a)**. The response signal of the sensor to 100 ppm NH_3 exhibited the highest value comparing with other single tested gases at 650 °C. The response values of the sensor to mixture gases consist of 100 ppm NH_3 and different concentrations of interference gas were close to the response to 100 ppm NH_3 at 650 °C. In order to more clearly elucidate quantificationally the selectivity of the fabricated sensor to different single interference gases, the selectivity coefficient denoted as K ($K = |R_{NH3}/ R_{other\ gas}|$) was introduced and shown in Fig. 6**(b)**. In this case, R_{NH3} represents the response value of the sensor to NH_3. $R_{other\ gas}$ is the response value to other gases. Here, $R_{NH3} = \Delta V_{NH3} = V_{NH3}\text{-}V_{air}$; $R_{other\ gas} = \Delta V_{other\ gas} = V_{other\ gas}\text{-}V_{air}$. The result demonstrated that the selectivity coefficient of the sensor to different single gases was from 27 to 340. And the change amplitude of the response value to coexistence gases was from 3.7% to 11.8%, which indicates the slight effect. Above results fully proved that the sensor utilizing $Cd_2V_2O_7$-SE exhibited the excellent selectivity to NH_3 at 650 °C. In order to explain reason for the excellent NH_3 selectivity of the sensor, the complex impedance characteristics of the device in air and various test gases including CH_4, CO, H_2, NO_2, NH_3 and mixture gases of NH_3 and NO_2 at 650 °C were measured and results are exhibited in Fig. 6**(c)**. As reported previously [39–41], the resistance at higher frequencies for the sensor is mainly associated with $Cd_2V_2O_7$-bulk resistance (including the small YSZ-bulk resistance). The interfacial resistance is given by the resistance value at the intersection of the large semi-arc with the real axis at lower frequencies (around 0.1 Hz). Clearly, the resistance at high frequencies was almost unchanged when the sensor was exposed to different tested gases. However, In the case of the sensor was exposed to 100 ppm NH_3, the interfacial resistance at the lower frequency was obviously decreased comparing with that of the sensor tested in other measured gases. Changes in the interface resistance in different target gases revealed the electrochemical catalytic activity towards the examined gas species. Thus, it can be speculated that the catalytic activity to the electrochemical reaction of NH_3 for present sensor at TPB was high, which generated the largest sensing characteristic toward NH_3. Additionally, the complex impedance of the sensor in mixture gases of 100 ppm NH_3 and 100 ppm NO_2 at 650 °C wasalso investigated. Obviously, the catalytic activity to the electrochemical reaction of coexistence gas at TPB is slightly higher than that of 100 ppm NH_3, which is certainly consistent with the change result in response value.

The good resistance to humidity and long term high temperature test are the prerequisite and crucial sensing performance evaluation parameter for the excellent gas sensing device. The effect of the relative humidity for the sensor attached with $Cd_2V_2O_7$-SE on response value at 650 °C is shown in Fig. 7**(a, b)**. The change of the response in different relative humidity for the sensor is denoted by the following equation: $\triangle V_h = [(\Delta V_a-\Delta V_0)/\Delta V_0 \times 100\%]$, where ΔV_a and ΔV_0 mean the response value of the sensor in a% and 55% RH, respectively. The change of response value for the sensor to 100 ppm NH_3 in different relative humidity range of 10–98% at 650 °C wasfrom –19% to 14%, which exhibited acceptable impact to NH_3 response characteristic in different relative humidity condition. Fig. 8 shows long-term stability of the sensor using $Cd_2V_2O_7$-SE to 100 ppm NH_3 at 650 °C. As indicated in Fig. 8**(a)**, the base line potential and response potential of the sensor attached with $Cd_2V_2O_7$-SE displayed a minor degree of potential fluctuation at continuous high temperature of 650 °C during 30 days measurement. The change of the ΔV ($\triangle V_s$) for the sensor is given by

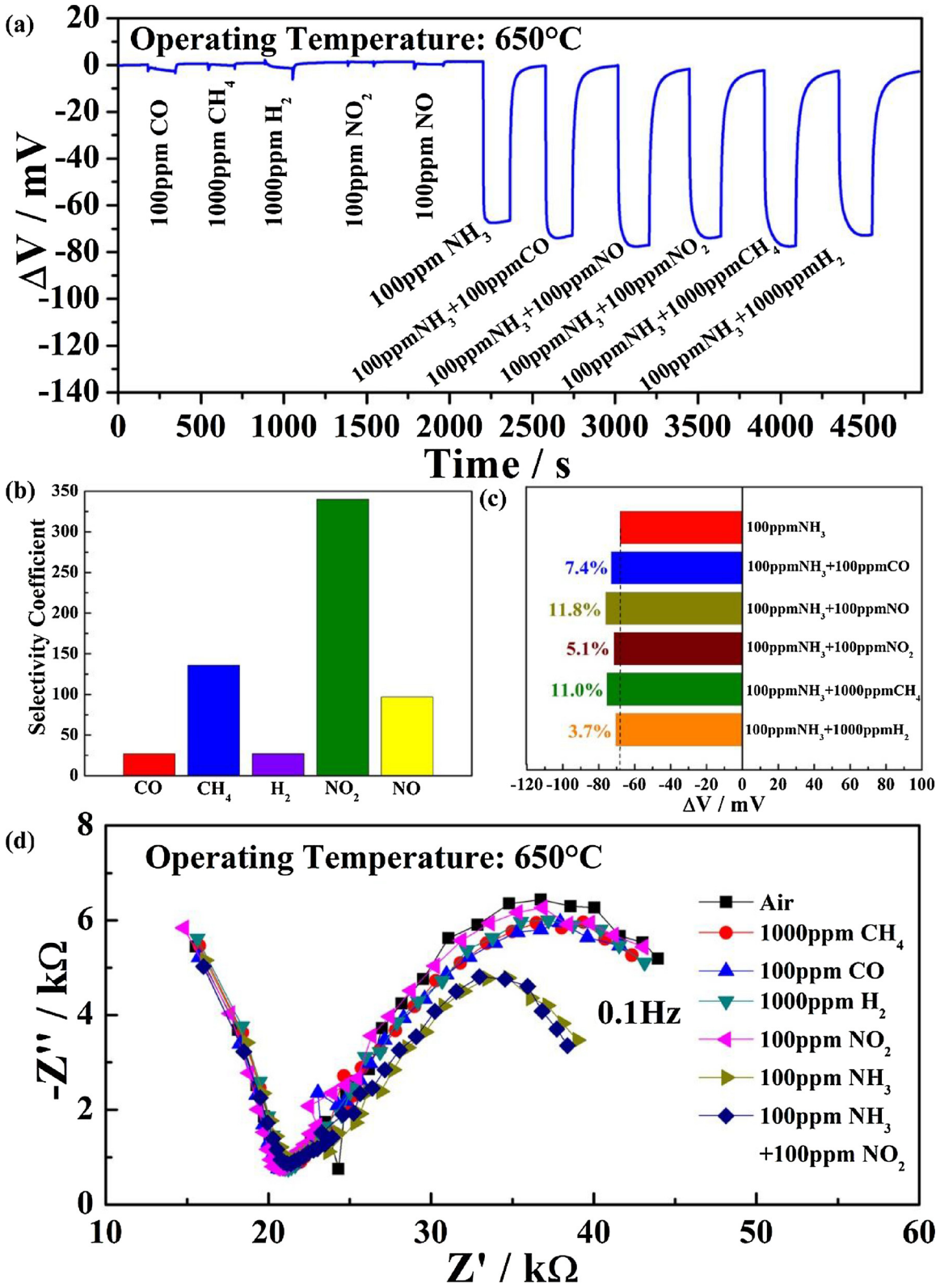

Fig. 6. (a) Response and recovery curves of the sensor attached with $Cd_2V_2O_7$-SE to various gases at 650 °C; (b) The selectivity coefficient of the sensor to tested gases; (c) Cross-sensitivities of the sensor to 100 ppm NH_3 and coexistence of gases; (d) Complex impedance curves of the present sensor in various tested gases at 650 °C.

$\triangle V_s = [(\Delta V_n - \Delta V_0)/\Delta V_0 \times 100\%]$, where ΔV_n and ΔV_0 denote the ΔV of the sensor on the n and initial day, respectively. The attenuation amplitude of response signal value for the fabricated sensor to 100 ppm NH_3 on 30th day at 650 °C was–1.5%, and the response characteristics of the sensor to 100 ppm NH_3 on initial, 10th, 20th and 30th day exhibited relative good concordance at 650 °C (Fig. 8**(b)**). Furthermore, the sensing performance of the fabricated device after 30 days measurement of 650 °C wasevaluated to further investigate stability. The dependence of

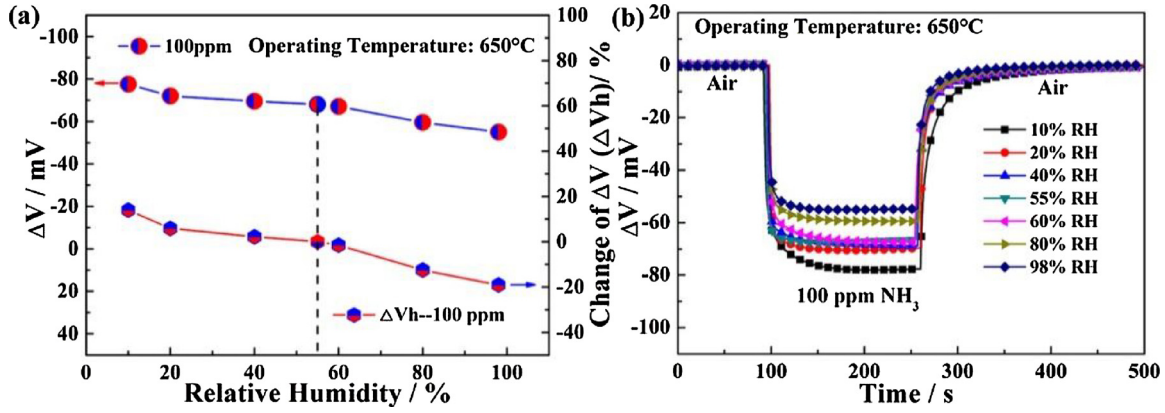

Fig. 7. (a) Effect of the relative humidity on response values at 650 °C; (b) Response and recovery curves of the sensor to 100 ppm NH_3 at different relative humidity.

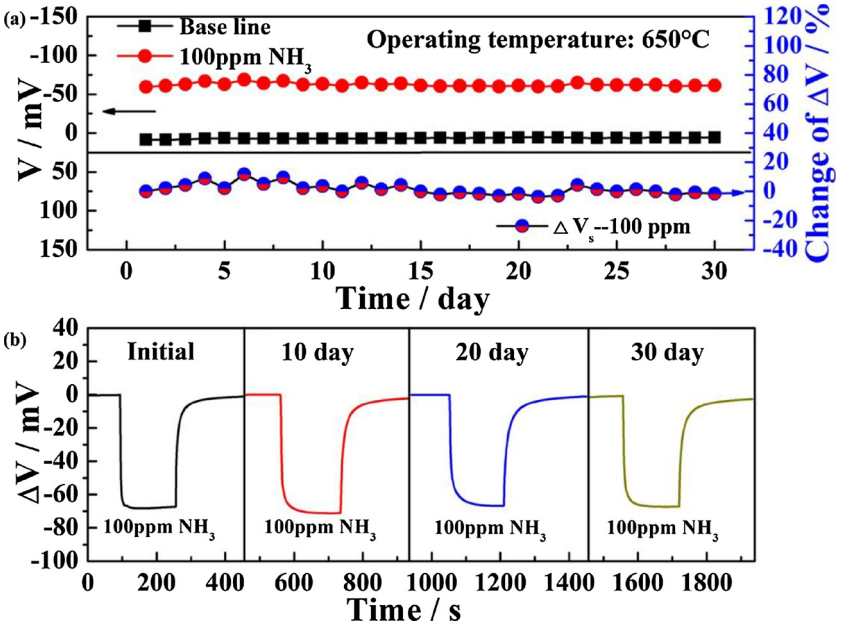

Fig. 8. (a) Long-term stability of the sensor using $Cd_2V_2O_7$-SE to 100 ppm NH_3 at 650 °C; (b) Response and recovery curves of the sensor attached with $Cd_2V_2O_7$-SE to 100 ppm NH_3 on initial, 10th, 20th and 30th day at 650 °C.

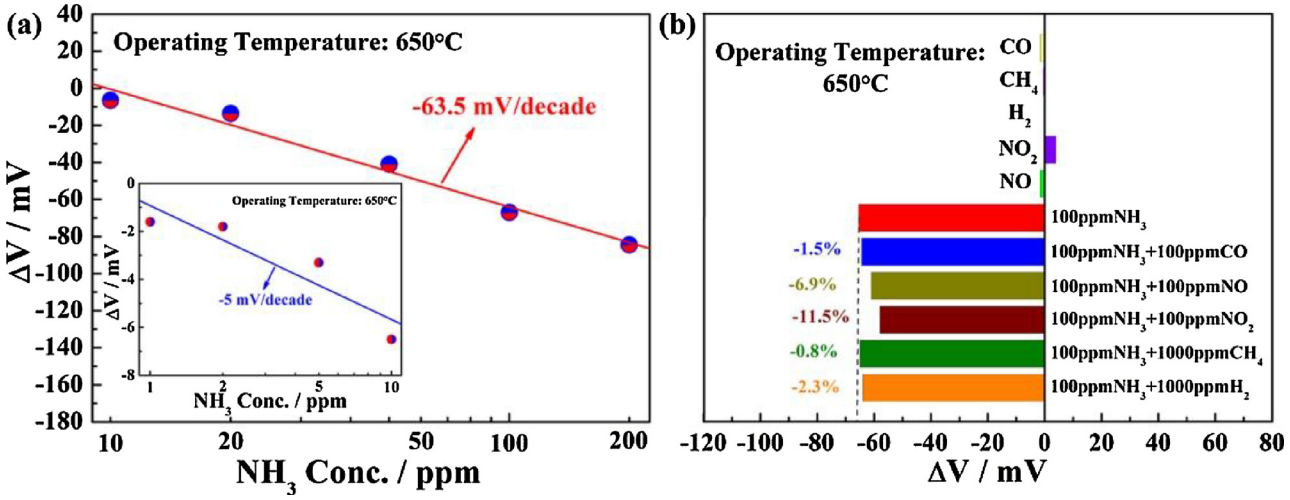

Fig. 9. (a) Dependence of ΔV on the logarithm of NH_3 concentrations and (b) the cross sensitivities for the sensor after 30 days measurement of 650 °C.

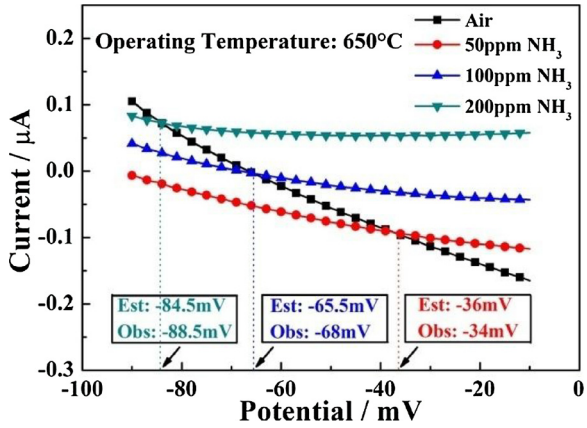

Fig. 10. Modified polarization curves for the sensor attached with $Cd_2V_2O_7$-SE in air, 50, 100 and 200 ppm NH_3 at 650 °C.

ΔV on the logarithm of NH_3 concentrations and the cross sensitivities for the developed sensor after 30 days high temperature measurement of 650 °C were tested and results depicted in Fig. 9. As indicated in Fig. 9**(a)**, the present sensor still achieved the low detection limit of 1 ppm NH_3 and displayed the segmented linear relationship between response value and logarithm of NH_3 concentration in the range of 1–200 ppm, which the sensitivities were –5 (1–10 ppm) and –63.5 mV/decade (10–200 ppm), respectively. The sensitivities of the sensor to NH_3 decreased by 1 mV/decade in the range of 1–10 ppm and 2.5 mV/decade in the range of 10–200 ppm after 30 days measurement of 650 °C, which demonstrated the slight attenuation in sensitivity. Additionally, it can be seen from Fig. 9**(b)** that the developed sensor also exhibited excellent selectivity to single and mixture of interference gases after 30 days measurement of 650 °C. Based on above obtained results, the developed sensor based on YSZ and $Cd_2V_2O_7$-SE revealed the extensive application prospect in detection of NH_3 at high temperature.

Furthermore, the polarization curves of the device attached with $Cd_2V_2O_7$-SE in air and different concentrations of NH_3 were measured to verify the sensing mechanism involving mixed potential model. The modified cathodic polarization curve was obtained in air, and the modified anodic polarization curve was obtained by subtracting in air from in different concentrations of tested sample gases. As reported in literatures [11,42,43], the mixed potential values of the sensor can be estimated from the intersection of the anodic and cathodic polarization curves. As displayed in Fig. 10, the mixed potential estimated values (–36, –65.5 and –84.5 mV) of the fabricated sensor to 50, 100 and 200 ppm NH_3 were similar to the response values (−34, −68 and −88.5 mV) experimentally observed at 650 °C, indicating that the developed device abided by the mixed potential sensing mechanism.

The present YSZ-based mixed potential type NH_3 sensor attached with $Cd_2V_2O_7$- SE is composed of the following electrochemical cell:

In air: air, $Cd_2V_2O_7$-SE/YSZ/Pt-RE, air

In sample gas: NH_3 (+air), $Cd_2V_2O_7$-SE/YSZ/Pt-RE, NH_3 (+air)

The electrochemical reactions for cathodic of O_2 and anodic of NH_3 proceeded concurrently at TPB of $Cd_2V_2O_7$-SE, target gas and YSZ solid electrolyte, which constructed a local cell. The potential difference between the SE and RE was measured as the potential response signal. In the case of two electrochemical reactions reached dynamic equilibrium, the mixed potential of the sensor was obtained.

$$\text{Anodic reaction: } 2/3\ NH_3 + O^{2-} \rightarrow 1/3\ N_2 + H_2O + 2e\text{-} \quad (4)$$

$$\text{Cathodic reaction: } 1/2\ O_2 + 2e^- \rightarrow O^{2-} \quad (5)$$

As has been done in previous research works [18,44,45], the mixed potential of the sensor can be treated quantitatively according to Butler-Volmer equation. The current densities for electrochemical reactions (4) and (5) can be expressed by Eqs. (6) and (7):

$$i_{NH_3} = i^0_{NH_3} \exp[2\alpha_1 F(V - V^0_{NH_3})/RT] \quad (6)$$

$$i_{O_2} = i^0_{O_2} \exp[-2\alpha_2 F(V - V^0_{O_2})/RT] \quad (7)$$

Where, i^0 and α are the exchange current density and transfer coefficient; F is the Faraday constant; V means the electrode potential; V^0 is the electrode potential at equilibrium; R and T represent the gas constant and temperature. We hypothesize that i^0 conforms to the following kinetic equations.

$$i^0_{NH_3} = B_1 C^n_{NH_3} \quad (8)$$

$$i^0_{O_2} = -B_2 C^m_{O_2} \quad (9)$$

Where, B_1, B_2, m and n are constant, C_{NH3} and C_{O2} are the concentration of NH_3 and O_2, $i^0_{NH_3}$ and $i^0_{O_2}$ are values with opposite signs. When the anodic and cathodic electrochemical reactions reach equilibrium, $i_{NH_3} + i_{O_2} = 0$ is established, and the mixed potential is expressed by V_M (ΔV):

$$V_M = V_0 + mA \ln C_{O_2} - nA \ln C_{NH_3} \quad (10)$$

Here,

$$V_0 = \frac{RT}{(2\alpha_1 + 2\alpha_2)F} \ln \frac{B_2}{B_1} + \frac{\alpha_1 V^0_{NH_3} + \alpha_2 V^0_{O_2}}{\alpha_1 + \alpha_2} \quad (11)$$

$$A = \frac{RT}{(2\alpha_1 + 2\alpha_2)F} \quad (12)$$

As depicted in Eq. (10), V_M varies negative linearly to the concentration logarithm of NH_3 ($\ln C_{NH3}$) at the fixed C_{O2} value, which has been demonstrated in Fig. 4**(c)**. Additionally, it can be observed from Fig. 4**(d)** that the response value to 100 ppm NH_3 displayed positive linear dependency with the logarithmic concentration of O_2, which was coincide with the result of Eq. (10) while the NH_3 concentration remains unchanged. Above theoretical analysis results and the experimental results achieved good consistence and these proved that the fabricated NH_3 sensor based on YSZ and $Cd_2V_2O_7$-SE conformed to the mixed potential sensing mechanism.

4. Conclusion

To sum up, the $Cd_2V_2O_7$ composite oxide sensing electrode material was synthesized by facile coprecipitation method and was first used for constructing the YSZ-based mixed potential type gas sensor aiming at achieving highly selective and stable NH_3 detection at high temperature. The XRD, Raman spectrum, XPS and FESEM demonstrated that the prepared sensing material was assigned to loose and porous pure monoclinic phase $Cd_2V_2O_7$ structure. Gas sensing measurement results indicated that the device attached with $Cd_2V_2O_7$-SE exhibited the low detection limit of 1 ppm to NH_3 and response value to 100 ppm NH_3 was −68 mV at 650 °C. The present device also displayed good reproducibility, acceptable humidity effect and long term stability to NH_3. The response value of the sensor to 100 ppm NH_3 decreased by 1.5% and the sensitivities to NH_3 decreased by 1 mV/decade in the range of 1–10 ppm and 2.5 mV/decade in the range of 10–200 ppm after 30 days high temperature measurement of 650 °C, respectively. The sensor also showed the excellent selectivity to NH_3 as oppose to single or coexistence interference gases before and after high temperature aging. Additionally, both the polarization curves and the theoretical analysis results demonstrated that the sensing mechanism of the developed sensor abided by mixed potential model. The $Cd_2V_2O_7$ material is a key component of high performance YSZ-based NH_3 sensor and the fabricated device involving in mixed potential mechanism presented the significant potential application value in field of on-board diagnosis for vehicle exhaust monitoring.

Acknowledgements

This work is supported by the National Nature Science Foundation of China (Nos. 61327804, 61520106003, 61374218, 61533021, 61474057, 61473132 and 61503148), Program for Chang Jiang Scholars and Innovative Research Team in University (No. IRT13018) and National High-Tech Research and Development Program of China (863 Program, No. 2014AA06A505), National Key Research and Development Program of China (Nos. 2016YFC0207300 and 2016YFC0201002), Application and Basic Research of Jilin Province (2013010 2010JC), High level scientific and technological innovation team of Jilin University (2017TD-07), The Fundamental Research Funds for the Central Universities.

References

[1] K. Li, L. Chen, S. White, H. Yu, X. Wu, X. Gao, M. Azzi, K. Cen, Smog chamber study of the role of NH_3 in new particle formation from photo-oxidation of aromatic hydrocarbons, Sci. Total Environ. 619-620 (2018) 927–937.
[2] S. Costa, J. Ferreira, C. Silveira, C. Costa, D. Lopes, H. Revas, C. Borrego, P. Roebeling, A. Miranda, J. Teixeira, Integrating health on air quality assessment–review report on health risks of two major European outdoor air pollutants: PM and NO_2, J. Toxicol. Environ. Health B Crit. Rev. 17 (2014) 307–340.
[3] K. Li, L. Chen, S. White, K. Han, B. Lv, K. Bao, X. Wu, X. Gao, M. Azzi, K. Cen, Effect of nitrogen oxides (NO and NO_2) and toluene on SO_2 photooxidation, nucleation and growth: a smog chamber study, Atmos. Res. 192 (2017) 38–47.
[4] Y. Jiang, C. Bao, Q. Liu, G. Liang, M. Lu, S. Ma, A novel CeO_2-MoO_3-WO_3/TiO_2 catalyst for selective catalytic reduction of NO with NH_3, Catal. Commun. 103 (2018) 96–100.
[5] R. Moos, D. Schönauer-Kamin, Review: recent developments in the field of automotive exhaust gas ammonia sensing, Sens. Lett. 6 (2008) 821–825.
[6] B. Timmer, W. Olthuis, A. Berg, Ammonia sensors and their applications-a review, Sens. Actuators B Chem. 107 (2005) 666–677.
[7] D. Schönauer, T. Nieder, K. Wiesner, M. Fleischer, R. Moos, Investigation of the electrode effects in mixed potential type ammonia exhaust gas sensors, Sens. Actuators B Chem. 192 (2011) 38–41.
[8] I. Lee, B. Jung, J. Park, C. Lee, J. Hwang, C. Park, Mixed potential NH_3 sensor with $LaCoO_3$ reference electrode, Sens. Actuators B Chem. 176 (2013) 966–970.
[9] C. Wang, X. Li, F. Xia, H. Zhang, J. Xiao, Effect of V_2O_5-content on electrode catalytic layer morphology and mixed potential ammonia sensor performance, Sens. Actuators B Chem. 223 (2016) 658–663.
[10] T. Sato, H. Ikeda, N. Miura, E.S.C. Electrochem, Mixed-potential type zirconia-based NH3 sensor using SnO_2-disk sensing electrode attached with sputtered Au, Lett. 3 (2014) B13–B15.
[11] B. Wang, S. Yao, F. Liu, Y. Guan, X. Hao, X. Liang, F. Liu, P. Sun, Y. Wang, H. Song, G. Lu, Fabrication of well-ordered porous array mounted with gold nanoparticles and enhanced sensing properties for mixed potential-type zirconia- based NH_3 sensor, Sens. Actuators B Chem. 243 (2017) 1081–1091.
[12] R. You, X. Hao, H. Yu, B. Wang, G. Lu, F. Liu, T. Cui, High performance mixed-potential-type zirconia-based NO_2 sensor with self-organizing surface structures fabricated by low energy ion beam etching, Sens. Actuators B Chem. 263 (2018) 445–451.
[13] T. Ritter, G. Hagen, J. Lattus, R. Moos, Solid state mixed-potential sensors as direct conversion sensors for automotive catalysts, Sens. Actuators B Chem. 255 (2018) 3025–3032.
[14] T. Ritter, G. Hagen, J. Kita, S. Wiegärtner, F. Schubert, R. Moos, Self-heated HTCC-based ceramic disc for mixed potential sensors and for direct conversion sensors for automotive catalysts, Sens. Actuators B Chem. 248 (2017) 793–802.
[15] P. Elumalai, V. Plashnitsa, Y. Fujio, N. Miura, Stabilized zirconia-based sensor attached with NiO/Au sensing electrode aiming for highly selective detection of ammonia in automobile exhausts, Electrochem. Solid-State Lett. 11 (2008) J79–J81.
[16] D. Schönauer, K. Wiesner, M. Fleischer, R. Moos, Selective mixed potential ammonia exhaust gas sensor, Sens. Actuators B Chem. 140 (2009) 585–590.
[17] Q. Diao, F. Yang, C. Yin, J. Li, S. Yang, X. Liang, G. Lu, Ammonia sensors based on stabilized zirconia and $CoWO_4$ sensing electrode, Solid State Ion. 225 (2012) 328–331.
[18] F. Liu, R. Sun, Y. Guan, X. Cheng, H. Zhang, Y. Guan, X. Liang, P. Sun, G. Lu, Mixed-potential type NH_3 sensor based on stabilized zirconia and $Ni_3V_2O_8$ sensing electrode, Sens. Actuators B Chem. 210 (2015) 795–802.
[19] Y. Yuan, B. Wang, C. Wang, X. Li, J. Huang, H. Zhang, F. Xia, J. Xiao, Effects of $CoFe_2O_4$ electrode microstructure on the sensing properties for mixed potential NH_3 sensor, Sens. Actuators B Chem. 462 (2017) 462–466.
[20] N. Markovic, P. Ross, Surface science studies of model fuel cell electrocatalysts, Surf. Sci. Rep. 45 (2002) 117–229.
[21] K. Shimizu, I. Chinzei, H. Nishiyama, S. Kakimoto, S. Sugaya, W. Matsutani, A. Satsuma, Doped-vanadium oxides as sensing materials for high temperature operative selective ammonia gas sensors, Sens. Actuators B Chem. 141 (2009) 410–416.
[22] F. Liu, Y. Wang, B. Wang, X. Yang, Q. Wang, X. Liang, P. Sun, X. Chuai, Y. Wang, G. Lu, Stabilized zirconia-based mixed potential type sensors utilizing $MnNb_2O_6$ sensing electrode for detection of low-concentration SO_2, Sens. Actuators B Chem. 238 (2017) 1024–1031.
[23] C. Wang, X. Cheng, X. Zhou, P. Sun, X. Hu, K. Shimanoe, G. Lu, N. Yamazoe, Hierarchical α-Fe_2O_3/NiO composites with a hollow structure for a gas sensor, ACS Appl. Mater. Interface 6 (2014) 12031–12037.
[24] R. Lewandowska, K. Krasowski, R. Bacewicz, J. Garbarczyk, Stusies of silver-vanadate superionic glasses using Raman spectroscopy, Solid State Ion. 119 (1999) 229–234.
[25] F. Hardcastle, I. Wachs, Determination of vanadium-oxygen bond distances and bond orders by Raman spectroscopy, J. Phys. Chem. 95 (1991) 5031–5041.
[26] R. Lozada-Morales, A. Cid-Garcial, G. López-Calzada, M.E. Zayas, O. Zelaya-Angel, J. Carmona-Rodriguez, E. Rubio-Rosas, R. Palomino-Merinol, O. Portillo-Moreno, S. Jiménez-Sandoval, Effect of Er-doping on the structural and optical properties of $Cd_2V_2O_7$, Physica Status Solidi A Appl. Res. 209 (2012) 2281–2285.
[27] P. Huang, X. Zhang, J. Wei, J. Pan, Y. Sheng, B. Feng, The preparation, characterization and optical properties of $Cd_2V_2O_7$ and $CdCO_3$ compounds, Mater. Chem. Phys. 147 (2014) 996–1002.
[28] B. Saha, R. Thapa, K. Chattopadhyay, Bandgap widening in highly conducting CdO thin film by Ti incorporation through radio frequency magnetron sputtering technique, Solid State Commun. 145 (2008) 33–37.
[29] S. Ni, X. Wang, G. Zhou, F. Yang, J. Wang, D. He, Crystallized $Zn_3(VO_4)_2$: synthesis, characterization and optical property, J. Alloys. Compd. 491 (2010) 378–381.
[30] M.-W. Kim, B. Joshi, H. Yoon, T. Ohm, K. Kim, S. Al-Deyab, S. Yoon, Electrosprayed copper hexaoxodivanadate (CuV_2O_6) and pyrovanadate ($Cu_2V_2O_7$) photoanodes for efficient solar water splitting, J. Alloys. Compd. 708 (2017) 444–450.
[31] J. Fergus, Sensing mechanism of non-equilibrium solid-electrolyte-based chemical sensors, J. Solid State Electrochem. 15 (2011) 971–984.
[32] N. Miura, T. Sato, S. Anggraini, H. Ikeda, S. Zhuiykov, A review of mixed- potential type zirconia-based gas sensors, Ionics 20 (2014) 901–925.
[33] S. Anggraini, Y. Fujio, H. Ikeda, N. Miura, YSZ-based sensor using Cr-Fe-based spinel-oxide electrodes for selective detection of CO, Anal. Chim. Acta 982 (2017) 176–184.
[34] X. Liang, S. Yang, J. Li, H. Zhang, Q. Diao, W. Zhao, G. Lu, Mixed-potential- type zirconia-based NO_2 sensor with high-performance three-phase boundary, Sens. Actuators B Chem. 158 (2011) 1–8.
[35] F. Liu, X. Yang, B. Wang, Y. Guan, X. Liang, P. Sun, G. Lu, High performance mixed potential type acetone sensor based on stabilized zirconia and $NiNb_2O_6$ sensing electrode, Sens. Actuators B Chem. 229 (2016) 200–208.
[36] S. Biswas, P. Pramanik, Studies on the gas sensing behaviour of nanosized $CuNb_2O_6$ towards ammonia, hydrogen and liquefied petroleum gas, Sens. Actuators B Chem. 133 (2008) 449–455.
[37] V. Srivastava, K. Jain, Highly sensitive NH_3 sensor using Pt catalyzed silica coating over WO_3 thick films, Sens. Actuators B Chem. 133 (2008) 46–52.
[38] A. Satsuma, M. Katagiri, S. Kakimoto, S. Sugaya, K. Shimizu, Effects of calcination temperature and acid-base properties on mixed potential ammonia sensors modified by metal oxides, Sensors 11 (2011) 2155–2165.
[39] N. Miura, M. Nakatou, S. Zhuiykov, Impedancemetric gas sensor based on zirconia solid electrolyte and oxide sensing electrode for detecting total NO_x at high temperature, Sens. Actuators B Chem. 93 (2003) 221–228.
[40] L. Wu, J. Xia, W. Shi, D. Jiang, Q. Li, NO_2-sensing properties of $La_{0.65}Sr_{0.35}MnO_3$ synthesized by self-propagating combustion, Ionics 22 (2016) 927–934.
[41] M. Stranzenbach, E. Gramckow, B. Saruhan, Planar, impedance-metric NO_x sensor with spinel-type SE for high temperature applications, Sens. Actuators B Chem. 127 (2007) 224–230.
[42] G. Lu, N. Miura, N. Yamazoe, Stabilized zirconia-based sensors using WO_3 electrode for detection of NO or NO_2, Sens. Actuators B Chem. 65 (2000) 125–127.
[43] G. Lu, N. Miura, N. Yamazoe, High-temperature sensors for NO and NO_2 based on stabilized zirconia and spinel-type oxide electrodes, J. Mater. Chem. 7 (1997) 1445–1449.
[44] N. Miura, S. Zhuiykov, T. Ono, M. Hasei, N. Yamazoe, Mixed potential type sensor using stabilized zirconia and $ZnFe_2O_4$ sensing electrode for NO_x detection at high temperature, Sens. Actuators B Chem. 83 (2002) 222–229.
[45] J. Zhang, C. Zhang, J. Xia, Q. Li, D. Jiang, X. Zheng, Mixed-potential NH_3 sensor based on $Ce_{0.8}Gd_{0.2}O_{1.9}$ solid electrolyte, Sens. Actuators B Chem. 249 (2017) 76–82.

Fangmeng Liu received his PhD degree in 2017 from College of Electronic Science and Engineering, Jilin University, China. Now he is a lecturer of Jilin University, China. His current research interests include the application of functional materials and development of solid state electrochemical gas sensor and flexible device.

Siqi Li received her M.S. degree from department of Chemical Engineering and Technology, Harbin Engineering University, China in 2016. Now, she is studying for her Ph.D. degree in College of Electronic Science and Engineering, Jilin University, China. She is engaged in the synthesis and characterization of organic/inorganic hybrid nanomaterials for gas sensor and development of flexible device.

Junming He received the B.Eng. degree in department of electronic science and technology in 2017. She is currently studying for her M.E. Sci. degree in College of Electronic Science and Engineering, Jilin University, China.

Jing Wang received her B.S. degree in applied chemistry in 2009 and the M.S. degree in polymer chemistry and physics in 2012 from Northeast Forestry University in China. Her current research is solid electrolyte gas sensor.

Rui You received his B.S. degree from Department of Opto-Electronic Engineering in 2013, Changchun University of Science and Technology, Changchun, China. He is now a Ph.D. student at the Department of Precision Instrument at Tsinghua University, Beijing, China. Currently his research interests mainly include gas sensor and application of MEMS process.

Zijie Yang received the B.S. degree in department of electronic science and technology in 2017. He is currently studying for his M.E. Sci. degree in College of Electronic Science and Engineering, Jilin University, China.

Lianjing Zhao received her M.S. degree in 2013 from Jilin University, China. She is currently studying for her Ph.D. degree in College of Electronic Science and Engineering, Jilin University. Her research interests mainly focus on the development of the functional nanomaterials and their applications in chem/biosensor.

Peng Sun received his PhD degree from the Electronics Science and Engineering department, Jilin University, China in 2014. Now, he is engaged in the synthesis and characterization of the semiconducting functional materials and gas sensors.

Xu Yan received his M.S. degree in 2013 from Nanjing Agricultural University. He joined the group of Prof. Xingguang Su at Jilin University and received his Ph.D. degree in June 2017. Since then, he did postdoctoral work with Prof. Geyu Lu. Currently, his research interests mainly focus on the development of the functional nanomaterials for chem/bio sensors.

Xishuang Liang received the B. Eng. degree in Department of Electronic Science and Technology in 2004. He received his Doctor's degree in College of Electronic Science and Engineering at Jilin University in 2009. Now he is an associate professor of Jilin University, China. His current research is solid electrolyte gas sensor.

Xiaohong Chuai is an associate professor and works in Department of Electrical Engineering, Jilin University, China. Her research interests are focused on sensor materials and devices.

Geyu Lu received the B.Sci. degree in electronic sciences in 1985 and the M.S. degree in 1988 from Jilin University in China and the Dr. Eng. degree in 1998 from Kyushu University in Japan. Now he is a professor of Jilin University, China. His current research interests include the development of chemical sensors and the application of the function materials.